Journal of Innovative Optical Health Sciences
Vol. 11, No. 6 (2018) 1850033 (12 pages)

DOI: 10.1142/S1793545818500335

Near-infrared laser irradiation of a multilayer agar-gel tissue phantom to induce thermal effect of traditional moxibustion

Jiyong Cho†
Department of Mechanical Engineering, Graduate School
Kookmin University, Seoul 02707, Republic of Korea
jiyong1224@nate.com

Bibin Prasad
Department of Radiation Oncology
SMG-Seoul National University Boramae Medical Center
Seoul 07061, Republic of Korea
bibinprasad07@gmail.com

Jung Kyung Kim*
School of Mechanical Engineering and
Department of Integrative Biomedical Science and Engineering
Graduate School, Kookmin University
Seoul 02707, Republic of Korea
jkkim@kookmin.ac.kr

Received 23 April 2018
Accepted 25 August 2018
Published 26 September 2018

Traditional moxibustion therapy can stimulate heat and blood-vessel expansion and advance blood circulation. In the present study, a novel noncontact-type thermal therapeutic system was developed using a near-infrared laser diode. The device allows direct interaction of infrared laser light with the skin, thereby facilitating a controlled temperature distribution on the skin and the deep tissues below the skin. While using a tissue-mimicking phantom as a substitute for real skin, the most important optical and thermal parameters are the absorption/attenuation coefficient, thermal conductivity, and specific heat. We found that these parameters can be manipulated by varying the agar-gel concentration. Hence, a multilayer tissue-mimicking phantom was fabricated using different agar-gel concentrations. Thermal imaging and thermocouples were used to measure the temperature distribution inside the phantom during laser irradiation. The temperature

*Corresponding author.
†Current address: RE-MEDI, Seoul 07203, Republic of Korea
Jiyong Cho and Bibin Prasad contributed equally to this work.

increased with the increase in the agar-gel concentration and reached a maximum value under the tissue phantom surface. To induce a similar thermal effect of moxibustion therapy, controlled laser-irradiation parameters such as output power, wavelength and pulse width were obtained from further analysis of the temperature distribution. From the known optothermal properties of the patient's skin, the temperature distribution inside the tissue was manipulated by optimizing the laser parameters. This study can contribute to patient-specific thermal therapy in clinics.

Keywords: Laser–tissue interaction; tissue phantom; moxibustion; hyperthermia; bioheat transfer.

1. Introduction

Thermal therapy is a treatment method used to control the physiological functions within an endurable temperature range and to maintain the local-tissue and whole-body temperature. In oriental medicine, moxibustion therapy is applied as a thermal treatment method. In general, moxibustion therapy cures or prevents diseases through heat stimulation by burning moxa, which comprises a herb named mugwort.[1] Thermal therapy is effective for treating diseases because it can enhance blood circulation by expanding the blood vessels. However, oriental doctors do not use this method as a routine clinical practice because of the pain from burns and unpleasant smoke and odor. Moreover, controlling the intensity of the applied heat during moxibustion therapy is difficult.[2,3] Moxibustion also has several disadvantages such as allergic reactions and polycyclic aromatic carcinogen production from a mugwort leaf that contains terpenes.[4,5]

The modern research on moxibustion is based on the radiation effects, thermal effects, and pharmacological actions of moxa. Infrared can produce nonthermal and thermal effects on a human body. Thermal effects are created under electromagnetic waves; hence, the tissues absorb energy to improve blood circulation.[4] Near-infrared laser is believed to have biological radiation effect on moxibustion as the light reflected by the skin is relatively low and can reach up to 10 mm deep in skin tissue.[6] Laser moxibustion offers the advantage of reducing pain. A study performed on rats using CO_2 laser moxibustion showed pain reduction in rats.[7] Studies also reported that infrared laser moxibustion could minimize cancer-related fatigue in a safe manner.[8]

To overcome the issues in the use of traditional moxibustion devices and to take advantage of laser moxibustion, a laser moxibustion device has been developed that employs an 830 nm diode-pumped solid-state (DPSS) infrared laser. The proposed device is free from smoke or odor. In addition, it does not induce skin burning because the device maintains a maximum temperature that is below that tolerable on the skin surface. Controlling the temperature on the skin surface and inside the deep tissues is an important factor that must be considered in thermal treatment. To obtain an optimal thermal effect in thermal therapy, the temperature inside the skin tissue and skin surface should be accurately controlled.[9,10] Many methods are available for measuring the temperature in the tissue phantom. The most effective method is temperature measurement using ultrasound waves or high-resolution thermal-imaging camera.[11,12] A method that uses a fiber-optic probe, which is nonmetallic and nonelectrical in nature, can be used to measure the temperature in phantom and animal models.[13–16] In our previous research, we developed a technique for temperature measurement inside a deep tissue heated by an infrared laser to test the efficiency of a laser moxibustion device using a thermal-imaging camera and thermocouples.[17]

Various materials have been used as a substitute for skin in previous studies.[18–22] A multilayered phantom, which consists of the epidermis, dermis and subcutaneous layers, can be used to mimic skin tissues. The optothermal properties of each tissue layer are given[23]; however, obtaining appropriate phantom materials with similar properties is difficult. Therefore, the concentration of agar gel, which was used to mimic skin tissues, was controlled,[24–26] and the optical and thermal properties, which vary with different agar-gel concentrations, were determined. Then, we prepared phantoms consisting of three layers of agar gels with known optothermal properties and investigated the efficiency of the proposed laser moxibustion device using the fabricated tissue-mimicking skin phantom. Next, we

irradiated the different skin phantoms with infrared lasers, and the temperature distribution in the deep skin tissue was manipulated by controlling the laser moxibustion device parameters. Furthermore, the skin temperature was maintained in the range of 42–50°C to induce effective thermal stimulation for therapy.

2. Materials and Methods

2.1. *Measurement of attenuation coefficient*

The attenuation coefficient of the agar-gel phantom was measured at a laser wavelength of 830 nm. Tissue-mimicking phantoms were fabricated using different agar-gel concentrations of 0.5%, 1.5%, 2.5%, 3.5% and 5%. Then, the phantom models were used within 90 min of fabrication to prevent water evaporation. Figure 1(a) shows that a laser, a sample holder, and a power meter were arranged in a linear pattern using an optical rail. A 830 nm DPSS laser with 1 W of power was used for the measurement. Because the power meter was limited to an input power of less than 300 mW, a neutral density (ND) filter was positioned between the laser and sample holder. The intensity of the laser beam transmitted through the phantom and ND filter was measured using the power meter. The Lambert–Beer law was used to determine attenuation coefficient, $\mu(\mathrm{cm}^{-1})$, expressed as follows:

$$I = I_0 \exp(-\mu d), \tag{1}$$

where d (cm) is the phantom thickness, I_0 (W) is the intensity of the laser beam incident to the phantom, and I (W) is the intensity of the transmitted laser light.

2.2. *Measurement of specific heat*

The specific heat of the tissue phantom was measured to fabricate a phantom with a similar specific heat as that of actual skin. The phantom was placed in warm water, and its specific heat against the change in temperature was measured. Agar-gel was used as the phantom material. Figure 1(b) shows the specific-heat measurement for agar-gel concentrations of 1.5%, 2.5%, 3.5% and 5%. A polystyrene chamber was used for measurement to provide thermal insulation from the ambient surrounding. A glass beaker was placed inside the

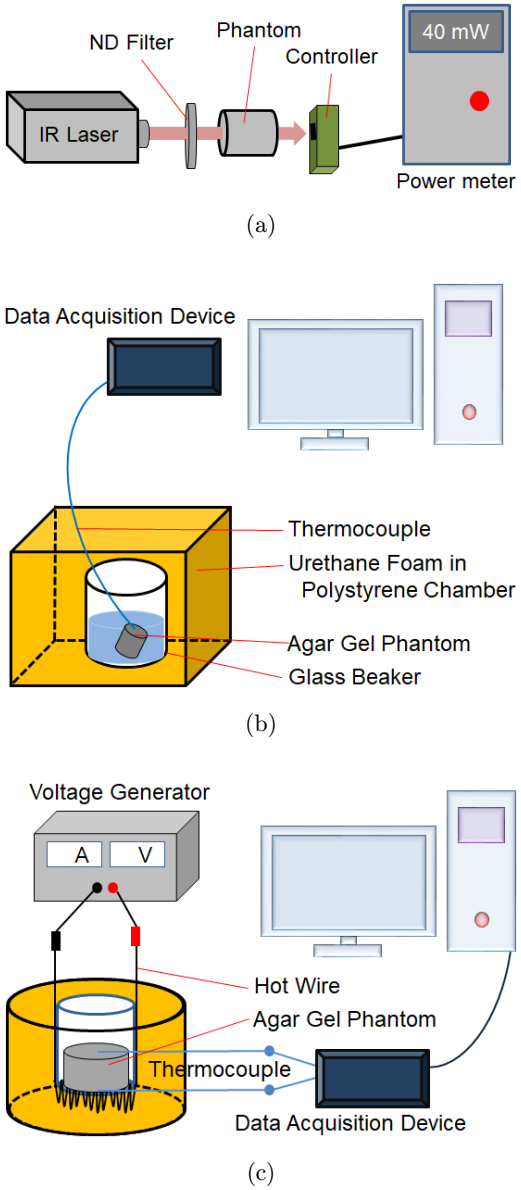

Fig. 1. Schematic of the measurement systems for (a) attenuation coefficient, (b) specific heat and (c) thermal conductivity of tissue phantom made of agar gel.

polystyrene chamber, and a urethane foam spray was used for insulation. When the agar-gel phantom and water were added to the beaker, the heat loss caused by the warm water (Q_{water}) was assumed to be equal to the heat gained by the glass beaker (Q_{beaker}) and the agar-gel phantom (Q_{phantom}) as follows:

$$Q_{\mathrm{water}} = Q_{\mathrm{beaker}} + Q_{\mathrm{phantom}}. \tag{2}$$

The specific-heat values of water and glass beaker were known. The mass of the glass beaker, warm water and agar-gel phantom was measured before

the experiment was performed. Before and after the experiment, the changes in the temperature of the glass beaker, water and agar-gel phantom were measured. Then, the specific heat of the agar-gel phantom was calculated as follows:

$$C_{\text{phantom}} = \frac{C_{\text{water}} m_{\text{water}} \Delta T_{\text{water}} - C_{\text{beaker}} m_{\text{beaker}} \Delta T_{\text{beaker}}}{m_{\text{phantom}} \Delta T_{\text{phantom}}}, \quad (3)$$

where m and C denote the mass and specific heat, respectively.

2.3. *Measurement of thermal conductivity*

The thermal conductivity of the agar-gel phantom was measured using the hot-wire method. As shown in Fig. 1(c), a hot wire was coiled at the bottom of the sample holder, and heat flux was supplied to the phantom. Then, polystyrene was placed under the hot wire using urethane foam spray, which ensured that the area surrounding the sample holder was adiabatic. The heat flux was controlled by supplying voltage to one side of the agar-gel phantom using the hot wire, and heat was transferred to the other side of the phantom. Next, the thermal conductivity of the phantom was calculated using the temperature difference of the phantom as follows:

$$Q = \frac{kA(T_1 - T_2)}{L}, \quad (4)$$

where L is the thickness of the phantom, A is the area of the phantom, T_1 is the temperature at the heat-receiving side and T_2 is the temperature at the opposite side. The hot-wire resistance was 4.3 Ω, and the supplied voltage was 5 V.

2.4. *Fabrication of skin-tissue phantom*

Human skin comprises three layers — the epidermis, dermis and subcutaneous tissue — and their thermal properties differ. A tissue phantom was fabricated with three layers based on the attenuation coefficient, thermal conductivity and specific heat of the phantom material. The agar solution was placed in an acrylic sample holder that was developed in our previous research.[17] The solution was solidified to form a gel. First, we poured the agar solution in the sample holder to form the bottom layer. After solidification of the agar solution, an agar solution with a different concentration was poured over the previous agar solution layer to form the middle layer. Finally, a third agar solution with a different concentration was poured over the middle layer to form the top layer. Figure 2(a) shows that the agar solutions in all three layers solidified to form a multilayered phantom. The composition of the agar-gel tissue phantoms fabricated to measure the temperature distribution is listed in Table 1.

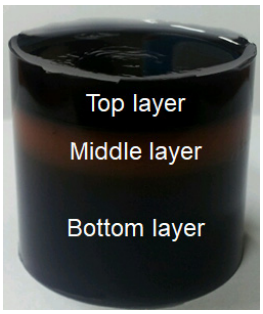

(a)

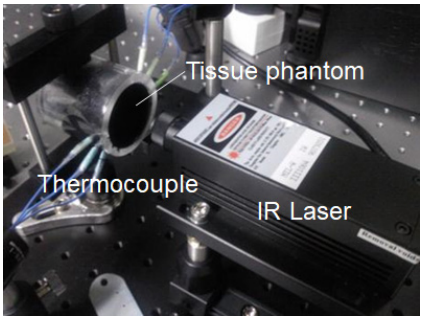

(b)

Fig. 2. (a) Multilayer agar gel phantom and (b) Sample holder with thermocouples inserted into the tissue phantom irradiated by infrared laser.

Table 1. Compositions of agar-gel tissue phantoms used herein.

Phantom / Layer	P1	P2	P3	P4
	Agar-gel concentration (%)			
Top	5	0.5	0.5	1.5
Middle	2.5	1.5	1.5	0.5
Bottom	0.5	0.5	5	5

2.5. *Measurement of temperature distribution*

In general, the human-skin thickness is ∼4 mm (including the epidermis and dermis). During moxibustion therapy, oriental doctors apply thermal stimulation to the blood vessels in the subcutaneous tissue. Thus, the temperature distribution at a depth of 4 mm in the phantom was measured, which was the distance of the subcutaneous tissue from the skin surface. A constant-temperature chamber was used to measure the temperature distribution. The temperature inside the chamber was maintained at 30°C during the experiment. The sample holder and laser controller were fixed in the chamber. The cylindrical sample holder had holes on the surface at fixed intervals. The internal temperature distribution was measured using thermocouples inserted through these holes in the phantom. In some cases, when the infrared laser irradiated the phantom, a rapid increase in the temperature of the phantom was observed because of the scattering of light due to the bumping thermocouple. Thus, to overcome this problem, thermocouples made of thin needles were used. The experimental setup is shown in Fig. 2(b).

The phantom sample in the sample holder was heated via laser irradiation. A continuous-wave laser beam was used. A thermocouple was used to measure the internal temperature of the heated phantom, and the measurement data were extracted using a data acquisition (DAQ) device that comprised two modules (NI 9211, National Instruments, USA) inserted into a compact DAQ chassis (NI cDAQ-9174, National Instruments, USA). Finally, the data were organized using DAQ software (LabVIEW 2009, National Instruments, USA). The distance between the sample and laser was 10 mm, and a laser irradiation power of 1 W was used. We measured the temperature inside the four types of phantoms, and the results were compared.

2.6. *Temperature distribution confirmed via thermal imaging*

We assumed that the temperature distributions will be different because the samples comprised three layers with different optical and thermal properties. The temperature distribution was visualized using a thermal-imaging camera (MobIR® M8, NewTech Instruments, Korea). An 830-nm infrared laser was used to heat the phantom based on the attenuation coefficient, specific heat, and thermal conductivity of the three layers. An infrared thermal-imaging camera can measure only the surface temperature and cannot measure the internal temperature distribution of an object. Therefore, the existing sample holder was modified. We cut off the upper parts of the sample and the sample holder to expose the core region to measure the temperature distribution inside the sample, similar to that performed in our previous study.[17] The thermal images of the phantom irradiated from above by the laser were captured using the thermal-imaging camera.

2.7. *Performance test of the laser moxibustion device*

The performance of the proposed laser moxibustion device was tested using the fabricated phantom. The distance between the phantom and the laser was 30 mm, and the laser power was fixed at 1 W. The temperature distribution inside the phantom was measured using the inserted thermocouples. In general, in moxibustion therapy, oriental doctors continuously burn several moxa samples to maintain a constant treatment temperature. The effective treatment temperature of the skin tissue in moxibustion therapy is typically assumed to be 42–50°C (5°C $\leq \Delta T \leq$13°C). To achieve this temperature in moxibustion, a mixed laser-irradiation method with pulsed and continuous waves was used. The laser was irradiated in a continuous-wave mode for the first 30 s, used in the pulse-wave mode for 150 s, and stopped in the final 120 s. During the pulse-wave irradiation, the pulse width was controlled in a pulse level that ranged from 1 to 10. The laser was turned on for 5 s and turned off for 5 s at level 1. The laser irradiation time was increased by 0.5 s for each increase in the pulse level. Thus, at level 10, the phantom was irradiated by the laser for 9.5 s and was turned off for 0.5 s.

2.8. *Mathematical modeling and numerical simulation*

The experimental results obtained from this study were verified using numerical simulation. Previously, the temperature distribution inside the tissue during indirect moxibustion was computed by Jeon

and Choi[24] by solving an unsteady conjugate heat-transfer problem. Their major finding was that for an effective thermal stimulation, the depth of the zone should be ~5 mm.

In the present study, the assumption was that the heat generated (Q) due to the absorption of laser light inside the phantom exponentially decays with depth. Figure 3(a) shows that the phantom was divided into three layers with different optical and thermal properties. The numerical simulations in this study were performed using COMSOL Multiphysics (COMSOL, Inc., Burlington, MA, USA). The 3D physical model for the transient simulation is shown in Fig. 3(b). The temperature distribution was calculated using the heat transfer module by combining the Beer–Lambert law with the Pennes bio-heat-transfer equation. To obtain the temperature distribution in the phantom, only the heat conduction in solid without biological

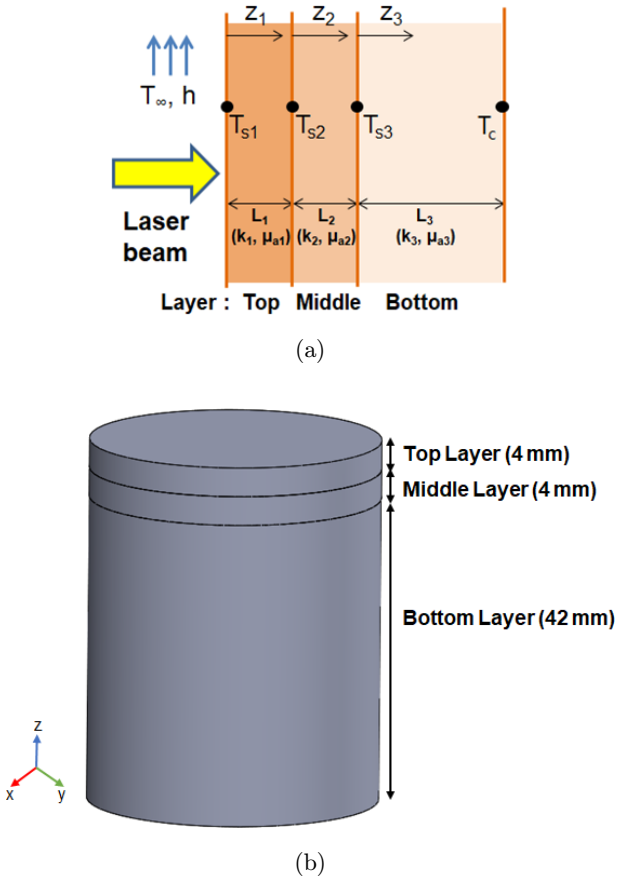

Fig. 3. (a) Schematic of the three-layer tissue phantom for the mathematical modeling of the temperature distribution and (b) 3D computational model used for simulation. The layers are assumed to have different optothermal properties.

parameters was considered. A user-defined function was provided as the laser-beam profile. The material properties used in the simulation are listed in Tables 2–4. The optical properties and thermal conductivity of skin are taken from previous study.[27,28] and specific heat, perfusion and metabolic heat generation are taken from IT'IS foundation.[29] Governing equation for the temperature distribution is expressed as follows:

$$\rho c \frac{\partial T}{\partial t} = \nabla \cdot (k \nabla T) - \rho_b c_b \omega_b (T - T_b) + Q_r + Q_m, \tag{5}$$

where Q_r is the heat-source term, which is equal to the absorbed light intensity multiplied by the absorption/attenuation coefficient of the medium, c is the specific heat of the medium, T is the temperature of the medium, k is the thermal conductivity of the medium, Q_m is the metabolic heat-generation rate in the medium, ω_b is the perfusion rate, and ρ_b, c_b, and T_b correspond to the density, specific heat, and temperature of the blood.

3. Results and Discussion

3.1. *Optical and thermal properties of the tissue phantom*

The measured attenuation coefficients of the agar-gel phantoms are listed in Table 2. The absorption coefficient of the human skin in the near-infrared wavelength is approximately 0.05–0.355 cm^{-1} (Refs. 30 and 31). Higher attenuation coefficients were found at higher concentrations of agar gel and ink. A multilayer tissue phantom with an

Table 2. Attenuation coefficient (cm^{-1}) according to the concentrations of agar-gel and ink.

Agar-gel concentration (%)	Ink concentration (%)	Attenuation coefficient (cm^{-1})
0.5	0.1	0.263
0.5	0.5	0.297
1.5	0.1	0.278
1.5	0.5	0.336
2.5	0.1	0.317
2.5	0.5	0.349
3.5	0.1	0.473
3.5	0.5	0.495
5	0.1	0.732
5	0.5	0.968

Table 3. Measured specific heat (J/kg · K) and thermal conductivity (W/m · K) at various concentrations of agar-gels used to fabricate skin tissue phantoms.

Agar concentration (%)	Specific heat (J/kg · K)	Thermal conductivity (W/m · K)
0.5	—	0.7449 ± 0.124
1.5	6465 ± 452	0.667 ± 0.116
2.5	5827 ± 218	0.591 ± 0.145
3.5	4887 ± 477	0.404 ± 0.171
5	4011 ± 386	0.379 ± 0.113

Table 4. Optical and thermal properties of human skin tissue.

Type of skin tissue	Absorption coefficient (cm^{-1})	Thermal conductivity (W/m·K)	Specific heat (J/kg·K)	Metabolic heat generation (W/kg)	Perfusion (mL/min/kg)
Epidermis	0.24	0.23	3391	1.65	106
Dermis	0.24	0.44	3391	1.65	106
Fat tissue	0.52	0.18	2348	0.51	33

attenuation coefficient comparable to that of human skin was prepared by adjusting the agar-gel concentration. Table 3 lists the measured thermal conductivity and specific heat values of the agar gels with various concentrations of agar. As the agar-gel concentration increased, the values of both properties decreased. The optical properties and thermal property values of the human skin tissue are listed in Table 4. Figure 4 shows the variation in the measured optical and thermal properties for different agar-gel concentrations.

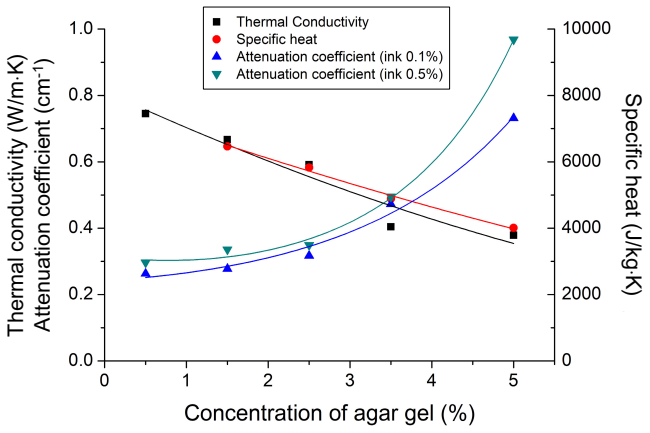

Fig. 4. Measured optical and thermal properties according to agar-gel concentration.

3.2. *Temperature distribution in the phantom irradiated by continuous-wave laser*

The four types of tissue phantom were irradiated with an 830 nm infrared laser. Figure 5 shows the temperature distribution in the agar phantom with different compositions of agar-gel layers with 0.1% ink. Figure 5(a) shows the temperature contours along the depth of the three-quarter phantom after 30 min time. We can see from the contours that as the concentration of the agar phantom varied, the temperature distribution in each layer was different. A high temperature increase was observed when the agar concentration was high in the bottom layer of the phantom (P3 and P4), whereas the other two phantoms (P1 and P2) showed a high temperature increase in the top layer. Figure 5(b) shows the comparison of the temperature increase that occurred at 4 mm below the surface of the four tissue phantoms after 30 min. The graph shows that the temperature measurement agreed with the simulation results with a slight variation, which confirms the measurement accuracy. It was also noted that the temperature increase in P2 was low because of the low agar concentration.

Figure 6 shows the temperature distribution in the agar phantom with different compositions of

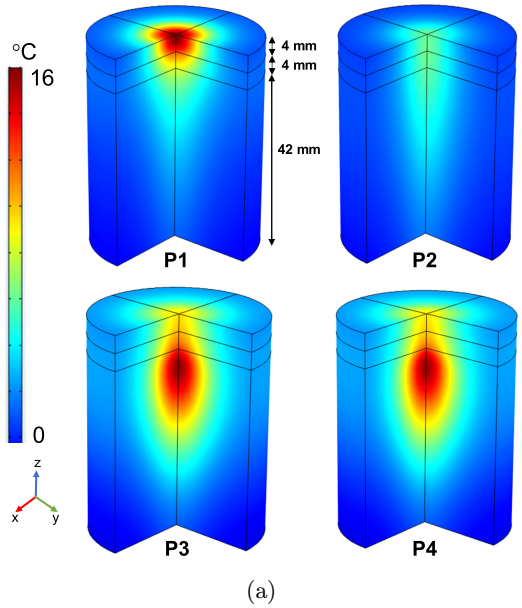

(a)

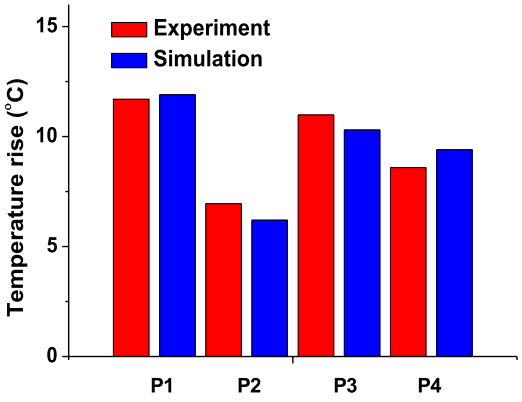

(b)

Fig. 5. (a) Temperature distribution along the depth of the three-quarter phantom with different concentration of agar with 0.1% ink after 30 min and (b) Comparison of temperature variations from experiment and simulation occurring 4 mm below the surface of phantoms with different compositions of agar gel layers after 30 min.

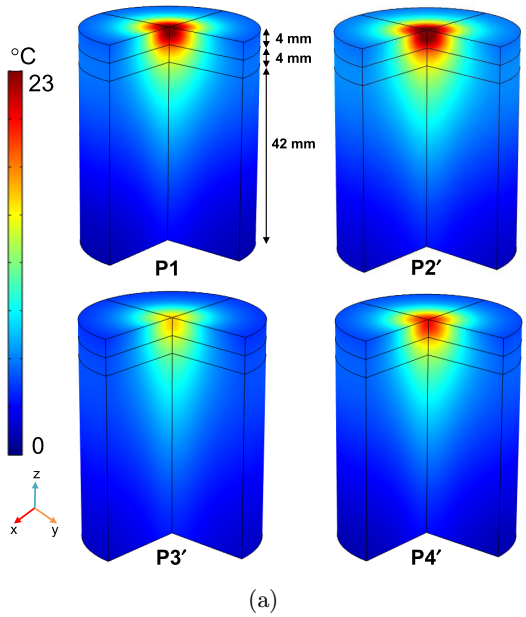

(a)

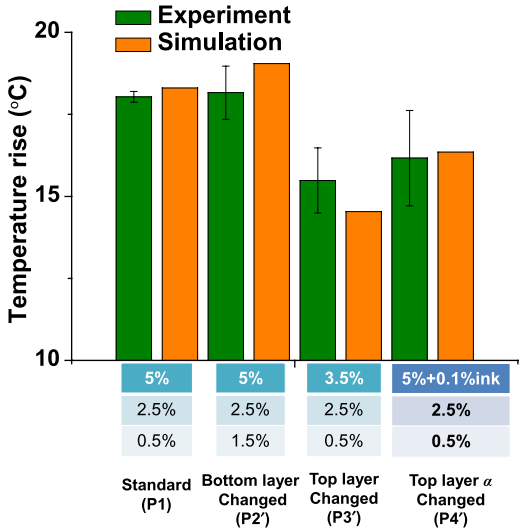

(b)

Fig. 6. (a) Temperature distribution along the depth of the three-quarter phantom with different concentration of agar with 0.5% ink after 2 h and (b) Comparison of temperature variations from experiment and simulation occurring 4 mm below the surface of phantoms with different compositions of agar gel layers with 0.5% ink after 2 h.

agar-gel layers with 0.5% ink. Figure 6(a) shows the temperature distribution contours along the depth of the three-quarter phantom. Because the concentration of agar was evidently high in the top layer, the temperature increase was higher toward the top layer. We also noted that the same agar-gel concentration with a low concentration of ink resulted in a smaller temperature increase than the high-concentration agar with ink. Figure 6(b) shows the comparison of the numerical and experimental temperature increase that occurred at 4 mm below the surface of the three-layer phantoms. The ranges of temperature increase in the experiments and simulation were found to agree. Overall, the temperature increase in each phantom layer was significantly affected by the optical and thermal parameters of the agar-gel. These results were based on the average of the results of the experiments conducted three times.

3.3. *Thermal imaging of the tissue phantom*

Four internal phantoms were investigated using a thermal-imaging camera. Figure 6 shows the thermal images of the internal temperature distributions of the four phantoms. The measured highest heat-source temperature was 31.3°C, as shown in Fig. 7(d), and the measured lowest heat-source temperature was 28.2°C, as shown in Fig. 7(b). As the agar-gel concentration increased, the temperature increased, which was similar to the temperature-measurement result obtained using a thermocouple. Our results confirmed that the optical properties in the top layer affects the temperature increase in the internal layers of the phantom. In addition, we found that the temperature in the bottom tissue layer changed because of the high concentration. Figures 7(c) and 7(d) show that the heat source was delivered to greater depths than that shown in Figs. 7(a) and 7(b). The bottom layers shown in Figs. 7(c) and 7(d) exhibited higher concentrations than those in the other cases. Finally, the results also show that producing a high temperature difference is possible if the specific heat of the material is varied. For thermal imaging, the removal of a small part of the agar-gel phantom can distort the core temperature distribution to some extent. Nevertheless, the overall trend of the depth-wise core temperature profile did not significantly change.

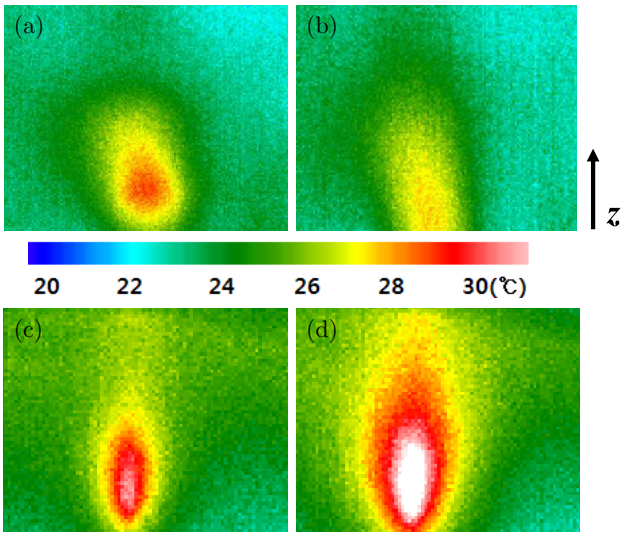

Fig. 7. Temperature distribution inside the tissue phantom visualized using a thermal imaging camera. The compositions of the agar gel layers are (a) P1, (b) P2, (c) P3 and (d) P4, as listed in Table 1.

3.4. *Performance test of the laser moxibustion device*

Figure 8(a) shows the temperature variations of the four phantoms heated using the laser moxibustion device at pulse level 7 for 25 min. For P1, we noted that the temperature increase was considerably high because the optical properties was highest at the top and middle layers of the phantom. According to these results, we confirmed that the phantom optical properties greatly affects its temperature. Figure 8(b) shows the internal temperature distribution due to the burning of commercial moxa at the phantom surface. The overall temperature variation shown in Fig. 8(a) is similar to that shown in Fig. 8(b). Thus, we determined that the proposed

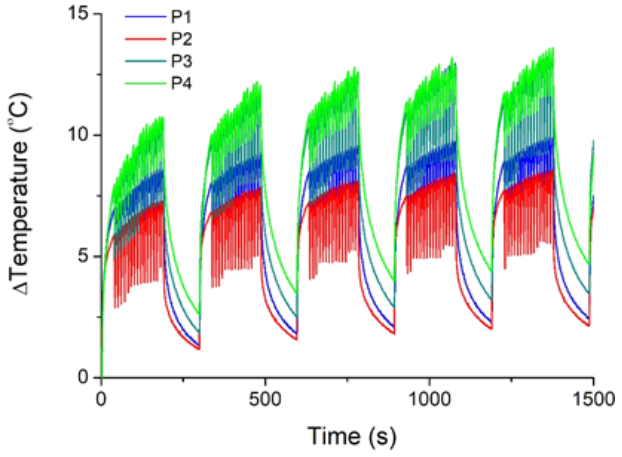

(a)

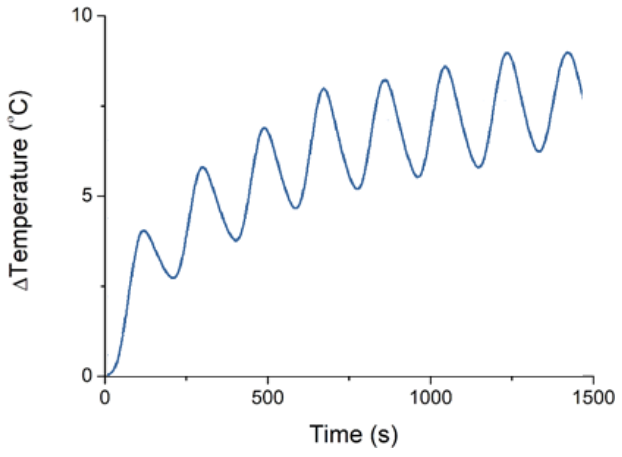

(b)

Fig. 8. (a) Temperature variations in tissue phantoms heated using the laser moxibustion device at pulse level 7 and (b) Temperature variation of the tissue phantom heated by burning commercial moxa.

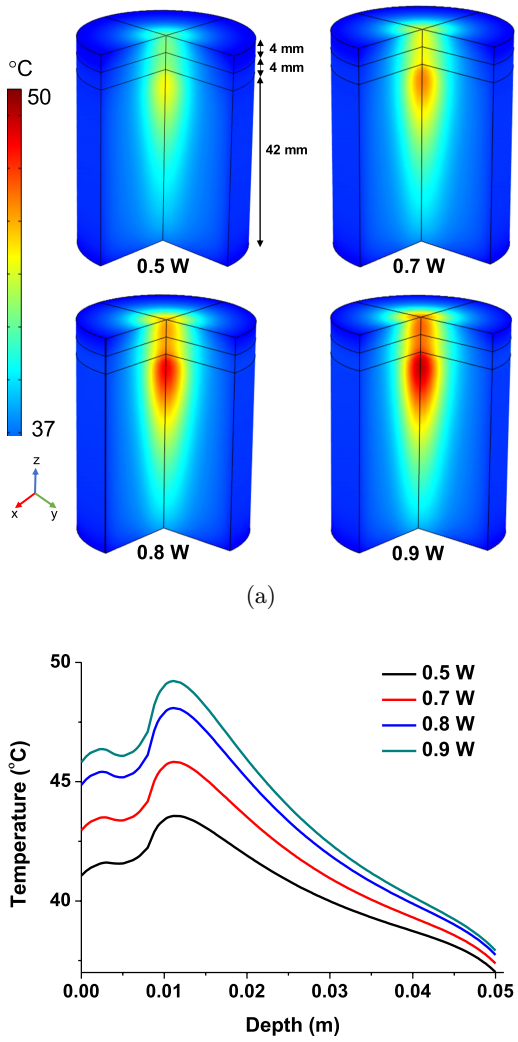

Fig. 9. (a) Temperature distribution along the depth of three-quarter skin tissue after 30 min laser irradiation and (b) Quantitative depth-wise temperature distribution along the skin tissue after 30 min laser irradiation.

laser moxibustion device could mimic the temperature distribution similar to that of a commercial moxa.

3.5. *Application of mathematical modeling to human-skin tissue*

Numerical simulations were performed to determine the temperature distribution in human-skin tissues considering thermal properties and physiological parameters such as perfusion and heat-generation rate. The optical and thermal properties of the human-skin tissue for simulation are listed in Table 4. The simulations were performed for an 830 nm laser irradiation on the multilayered skin tissue. The initial temperature of the three layers of the skin (epidermis, dermis, and fat) was assumed to be 37°C. Figure 9(a) shows the temperature distribution along the depth of the three layers of the three-quarter skin tissue after 30 min. A similar temperature profile was obtained when the laser power was varied and the temperature was controlled in the range of 42–50°C by modulating the laser output power. Figure 9(b) shows the depth-wise temperature distribution in the skin tissue after the laser irradiation. We confirmed that the temperature of the epidermis rapidly increased, which then caused a decrease in the temperature distribution in the dermis and a parabola-shaped increase in the temperature distribution in the fat tissues. The laser–tissue interaction is actively being studied, and the most important objective is to obtain the specific thermal effects without burning the skin-tissue surface under direct irradiation with a laser.[30,31] The present study demonstrated that precisely maintaining maximum temperature in the inner skin layer is possible by changing the laser output power. A large increase in temperature was observed just at the skin surface at high output power; hence, implementing a cooling process to prevent skin burning is advisable. Our results suggested that patient-specific thermal therapy can be realized by adjusting the laser parameters according to the known optothermal properties of the skin tissue of individuals.

4. Conclusion

The temperature distribution in a deep tissue phantom was controlled using various laser parameters. In addition, the optothermal properties such as the attenuation coefficient, specific heat, and thermal conductivity of an agar-gel tissue phantom, which depend on the agar concentration, were measured. A multilayer tissue phantom with known optical and thermal properties was fabricated using agar-gels with a concentration of 0.5%–5%. The temperature distribution inside the multilayer tissue phantom was predicted on the basis of experimental measurements and numerical simulation using the optothermal properties of each phantom layer, and the results obtained agreed well. The skin temperature could be regulated in the treatment temperature range between 42°C and 50°C by applying the actual skin-tissue parameters

using numerical simulation. Moreover, a temperature measurement system was developed using thermocouples that can measure the temperature distribution inside a laser-irradiated phantom. The temperature distribution inside the phantom was also determined using a thermal-imaging camera. Subsequently, a laser moxibustion device was developed on the basis of our experimental finding. The results suggest that to produce a specific temperature profile in the tissue, an optimal laser parameter set can be determined if the properties of the patient's skin tissue are known. By manipulating the temperature distribution inside the tissue through optimized laser parameters, we claim that personalized thermal therapy can be implemented in the future.

Conflict of Interest

Authors have no conflict of interest.

Acknowledgments

This study was supported by the National Research Foundation sponsored by the Ministry of Science, ICT and Future Planning (NRF-2016R1A2B4012095) and the Ministry of Education (NRF-2016R1D1A1A09917195), Republic of Korea.

References

1. J. R. Peterson, "Acupuncture in the 1990s," *Arch. Fam. Med.* **5**, 237–240 (1996).
2. J. Y. Cha, H. S. Myoung, S. P. Cho, K. J. Lee, "Development of deep-heating stimulation system for substituting the heat effect of moxibustion," *J. Inst. Electron. Eng. Korea* **46**, 50–57 (2009).
3. D. E. Yoon, B. K. Jo, "A study on the variations of the body trunk temperature by the drug-pad moxibustion method," *Trans. Kor. Inst. Elec. Engr.* **55**, 386–396 (2006).
4. H. Deng, X. Shen, "The Mechanism of Moxibustion: Ancient Theory and Modern Research," *Evid.-Based Complementary Altern. Med.* **2013**, 379291 (2013).
5. H. Li and S. Liu, "2 Cases of moxibustion allergy," *J. Tradit. Chin. Med.* **17**, 859–860 (2008).
6. A. Chiba, H. Nakanishi, S. Chichibu, "Thermal and antiradical properties of indirect moxibustion," *Am. J. Chin. Med.* **25**, 281–287 (1997).
7. F. Wu, R. Zhang, X. Shen, L. Lao, "Preliminary Study on Pain Reduction of Monosodium Iodoacetate-Induced Knee Osteoarthritis in Rats by Carbon Dioxide Laser Moxibustion," *Evid.-Based Complementary Altern. Med.* **2014**, 754304 (2014).
8. H. Mao, J. J. Mao, M. Guo, K. Cheng, J. Wei, X. Shen, X. Shen, "Effects of Infrared Laser Moxibustion on Cancer-Related Fatigue: A Randomized, Double-Blind, Placebo-Controlled Trial," *Cancer* **122**, 3667–3672 (2016).
9. B. Jung, C. S. Kim, B. Choi, J. S. Nelson, "Handheld pulsed photothermal radiometry system to estimate epidermal temperature rise during laser therapy," *Skin Res. Technol.* **12**, 292–297 (2006).
10. S. C. Gnyawali, Y. Chen, F. Wu, K. E. Bartels, J. P. Wicksted, H. Liu, C. K. Sen, W. R. Chen, "Temperature measurement on tissue surface during laser irradiation," *Med. Biol. Eng. Comput.* **46**, 159–168 (2008).
11. Y. Nawata, K. Kaneko, "Measurement of temperature distribution in phantom body by an ultrasonic CT method," *Proc. 5th ASME/JSME Joint Thermal Eng. Conf.* (1999).
12. M. Mital, E. P. Scott, "Thermal detection of embedded tumors using infrared imaging," *J. Biomech. Eng.* **129**, 33–39 (2007).
13. A. D. Reid, M. R. Gertner, M. D. Sherar, "Temperature measurement artefacts of thermocouples and fluoroptic probes during laser irradiation at 810 nm," *Phys. Med. Biol.* **46**, N149–N157 (2001).
14. M. T. Hossain, B. Prasad, K. S. Park, H. J. Lee, Y. H. Ha, S. K. Lee, J. K. Kim, "Simulation and experimental evaluation of selective heating characteristics of 13.56 MHz radiofrequency hyperthermia in phantom models," *Int. J. Precis. Eng. Manuf.* **17**, 253–256 (2016).
15. B. Prasad, Y. H. Ha, S. K. Lee, J. K. Kim, "Patient-specific simulation for selective liver tumor treatment with noninvasive radiofrequency hyperthermia," *J. Mech. Sci. Technol.* **30**, 5837–5845 (2016).
16. B. Prasad, S. Kim, W. Cho, S. Kim, J. K. Kim, "Effect of tumor properties on energy absorption, temperature mapping, and thermal dose in 13.56-MHz radiofrequency hyperthermia," *J. of Therm. Biol.* **74**, 281–289 (2018).
17. J. Cho, H. Byun, S. D. Lee, J. K. Kim, "Temperature distribution in deep tissue phantom during laser irradiation at 1,064 nm measured by thermocouples and thermal imaging technique," *J. Vis.* **14**, 265–272 (2011).
18. V. G. Liu, T. M. Cowan, S. W. Jeong, S. L. Jacques, E. C. Lemley, W. R. Chen, "Selective photothermal interaction using an 805-nm diode laser and indocyanine green in gel phantom and chicken breast tissue," *Lasers Med. Sci.* **17**, 272–279 (2002).
19. J. F. Burke, I. V. Yannas, W. C. Quinby Jr, C. C. Bondoc, W. K. Jung, "Successful use of a physiologically

acceptable artificial skin in the treatment of extensive burn injury," *Ann. Surg.* **194**, 413–428 (1981).
20. F. Manns, P. J. Milne, X. Gonzalez-Cirre, D. B. Denham, J. M. Parel, D. S. Robinson, "*In situ* temperature measurements with thermocouple probes during laser interstitial thermotherapy (LITT): Quantification and correction of a measurement artifact," *Lasers Surg. Med.* **23**, 94–103 (1998).
21. A. Robert, M. D. Weiss, "Comparison of endovenous radiofrequency versus 810 nm diode laser occlusion of large veins in an animal model," *Am. Soc. Dermatol. Surg.* **28**, 56–61 (2002).
22. I. Stadler, R. J. Lanzafame, R. Evans, V. Narayan, B. Dailey, N. Buehner, J. O. Naim, "830-nm irradiation increases the wound tensile strength in a diabetic murine model," *Lasers Surg. Med.* **28**, 220–226 (2001).
23. F. Xu, T. J. Lu, K. A. Seffen, E. Y. K. Ng, "Mathematical modeling of skin bioheat transfer," *Appl. Mech. Rev.* **62**, 1–35 (2009).
24. B. J. Jeon, H. G. Choi, "Heat-transfer analysis of indirect moxibustion using unsteady conjugate heat-transfer solutions," *J. Mech. Sci. Technol.* **24**, 2051–2057 (2010).
25. A. M. Elliott, A. M. Shetty, J. Wang, J. D. Hazle, R. J. Stafford, "Use of gold nanoshells to constrain and enhance laser thermal therapy of metastatic liver tumours," *Int. J. Hypertherm.* **26**, 434–440 (2010).
26. M. Zhang, Z. Che, J. Chen, H. Zhao, L. Yang, Z. Zhong, J. Lu, "Experimental determination of thermal conductivity of water-agar gel at different concentrations and temperatures," *J. Chem. Eng. Data* **56**, 859–864 (2011).
27. D. Haemmerich, D. J. Schutt, I. dos Santos, J. G. Webster, D. M. Mahvi, "Measurement of temperature-dependent specific heat of biological tissues," *Physiol. Meas.* **26**, 59–67 (2005).
28. I. S. Saidi, "Transcutaneous optical measurement of hyperbilirubinemia in neonates," Ph.D. Dissertation, Rice University, Houston, TX, USA (1992).
29. P. A. Hasgall, F. Di Gennaro, C. Baumgartner, E. Neufeld, B. Lloyd, M. C. Gosselin, D. Payne, A. Klingenböck, N. Kuster, "IT'IS Database for thermal and electromagnetic parameters of biological tissues," Version 4.0, www.itis.ethz.ch/database (2018).
30. A. Banerjee, A. A. Ogale, C. Das, K. Mitra, C. Subramanian, "Temperature distribution in different materials due to short pulse laser irradiation," *Heat Transfer Eng.* **26**, 41–49 (2007).
31. J. Jiao, Z. Guo, "Thermal interaction of short-pulsed laser focused beams with skin tissues," *Phys. Med. Biol.* **54**, 4225–4241 (2009).